Rigorous Evaluation of Losses in Uniform Leaky-Wave Antennas

Walter Fuscaldo, *Member, IEEE*

***Abstract*—General formulas are proposed for thoroughly evaluating the radiation efficiency of traveling-wave antennas operating in any radiating regime. Indeed, existing theoretical models only work in the scanned-beam region, where the radiating mode is considerably above cutoff and the perturbation method applies. The analysis provided here extends the application of the perturbation method close to the cutoff condition, thus providing a correct estimation of the losses even in the case of broadside radiation. This case is particularly important for Fabry-Perot cavity leaky-wave antennas (FPC-LWAs) based on partially reflecting screens (PRSs), which are commonly designed to generate a broadside pencil beam. However, previous works on FPC-LWAs always assume either a lossless PRS, or a lossless dielectric cover layer thus neglecting metal and dielectric losses: a hypothesis that is no longer fulfilled at high frequencies, such as millimeter-wave and submillimeter-wave frequencies. An original theoretical framework is thus developed to derive analytical formulas for a rigorous evaluation of losses when either lossy PRS or lossy dielectric cover layers are employed. Interestingly, the equivalence between a lossy PRS and a lossy dielectric cover layer is shown from a theoretical viewpoint. All the findings derived here are validated through full-wave simulations to corroborate the proposed analysis.**

***Index Terms*—Leaky-wave antennas (LWAs), leaky waves, Fabry-Perot cavity antennas, terahertz, metasurfaces, frequency selective surfaces.**

I. Introduction

THE modern society is experiencing a growing need of being connected with multiple technological devices, a concept that is well expressed by the so-called Internet of Things (IoT). Most of the real-world IoT applications are calling for reliable, secure and real-time communications [1]. As a result, the emerging 5G wireless paradigm is shifting from microwave frequencies to millimeter-wave and even sub-millimeter-wave frequencies. As shown in [2], high data-rate channels for future IoT real-world applications will demand bandwidths on the order of tens of GHz, a requirement that is permitted only at frequencies as high as 300 GHz, due to the band limitations dictated by the current spectrum usage regulations.

For this purpose, a particular class of radiating elements, namely Fabry-Perot cavity leaky-wave antennas (FPC-LWAs) [3] has recently been proposed at millimeter-wave frequencies as promising platforms for future 5G antenna systems [4]–[6] and at sub-millimeter frequencies for THz indoor wireless communications [7]–[9]. Among other high-frequency antenna solutions (see e.g., [10] and refs. therein), FPC-LWAs have the advantage of being fully planar, cost-effective, and highly directive. The typical architecture of a FPC-LWA consists of a grounded dielectric substrate covered with a partially reflecting surface (PRS). In particular, in the THz range, the choice of the dielectric material and the PRS realization is subjected to several constraints dictated by THz technology, as extensively commented in [9]. Some recent examples of THz FPC-LWAs are those based on graphene, fishnet-like unit-cells, and nematic liquid crystals [10].

Theoretical models for evaluating the radiating features of such FPC-LWAs exist [11]. However, two issues arise when one needs to analytically evaluate the radiation efficiency of a FPC-LWA radiating at broadside. The first issue is related to the *broadside condition*. As a matter of fact, current techniques for evaluating the radiation efficiency of LWAs assume that the antenna radiates a scanned beam [12], [13]. The second issue is related to the *circuit modeling* of an FPC-LWA. Indeed, available formulas for the radiating features of FPC-LWAs model the PRS as a lossless impedance, thus neglecting both dielectric and metal losses. However, these losses are no longer negligible at high frequencies, and might be particularly relevant for certain materials at THz, thus considerably affecting the antenna performance.

In this work we have a twofold objective. First, we aim at extending the original work in [12] for the evaluation of losses in 1-D uniform unidirectional LWAs radiating a scanned beam, to the case of either 1-D uniform bidirectional, or 2-D uniform LWAs radiating at broadside. Second, we aim at extending the theoretical model originally developed in [11] for 2-D uniform FPC-LWAs based on *lossless* PRSs to the *lossy* case. This investigation furnishes closed-form expressions for an accurate evaluation of the radiating performance of FPC-LWAs based on lossy PRS. Moreover, the possibility to model a *lossy dielectric cover layer* with an equivalent *lossy PRS* is discussed as well, thus extending the equivalence between substrate-superstrate LWAs and PRS-like FPC-LWAs established in [14] for the *lossless* case only.

All the results reported in this work have been supported through full-wave simulations in different operating conditions. It is worth mentioning here that a full-wave simulation of a directive THz FPC-LWA is considerably expensive in terms of computational resources, due to the *electrically-large dimensions* involved and the *resonant character* of the structure. This aspect further motivates the importance of analytical techniques for the accurate evaluation of the radiating performance of this class of structures. Finally, three case studies are presented. A graphene-based FPC-LWA and a substrate-superstrate FPC-LWA, to show the possible applications to THz antenna design, and a more conventional FPC-

Manuscript received XXX. xx^xx, xxxx

W. Fuscaldo is with the Department of Information Engineering, Electronics and Telecommunications, Sapienza University of Rome, 00184 Rome, Italy. (email: walter.fuscaldo@uniroma1.it).

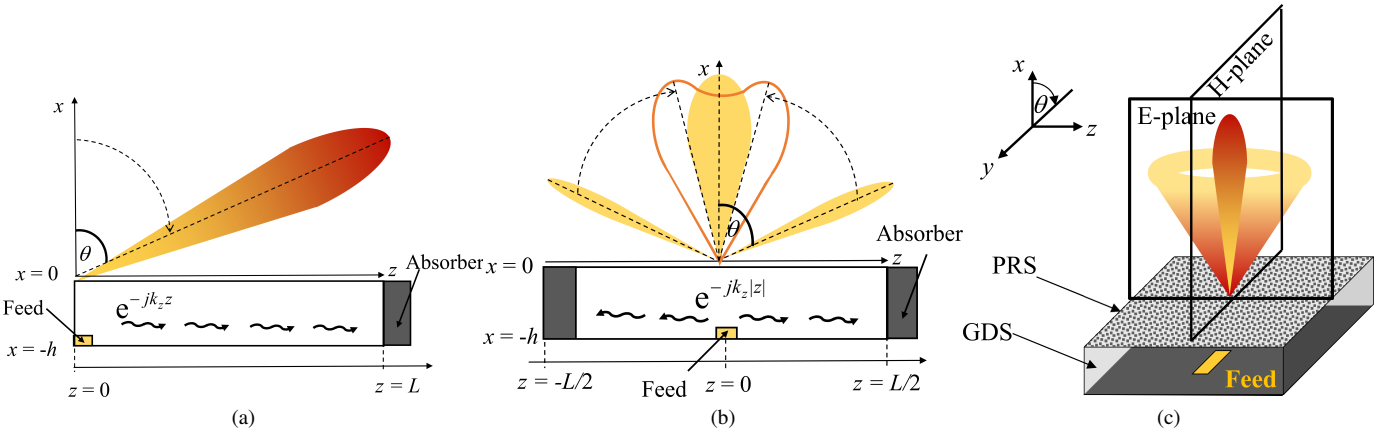

Fig. 1. (a)–(c) Illustrative examples of different LWAs. (a) A 1-D unidirectional LWA radiating a scanned beam. (b) A 1-D bidirectional LWA radiating two scanned beams that can merge at broadside to produce a single broadside beam. (c) A 2-D uniform FPC-LWA that is capable of radiating either a conical beam or a broadside pencil beam.

LWA based on homogenized PRS, to show the application of the formulas when commercial lossy laminates are employed in the microwave range.

The manuscript is organized as follows. In Section II, a theoretical analysis is developed to derive new formulas for the evaluation of losses in 1-D uniform LWAs radiating at broadside. This analysis also applies to the case of 2-D uniform LWAs. Therefore, from this result we move on the analysis of FPC-LWAs radiating at broadside. After reviewing the properties of FPC-LWAs based on lossless PRSs, the theoretical model is extended to account for the case of lossy PRSs. The equivalence between FPC-LWAs based on lossy PRS and those based on lossy superstrates is also discussed to further extends the applicability of the results. In Section III, all the original formulas are validated through full-wave simulations to clearly assess their consistency and accuracy. In Section IV, the proposed formulas are applied for the evaluation of the radiating properties of two different THz FPC-LWAs, and a more conventional microwave FPC-LWA. Finally, conclusions are drawn in Section V.

II. Theoretical Analysis

This Section II is split into two Subsections. Subsection II.A extends the formula originally reported in [12] for the radiation efficiency of traveling-wave antennas radiating a scanned beam, to the case of broadside radiation. Subsection II.B focuses on the radiating features of FPC-LWAs. The fundamental properties of this specific class of structures have been derived in [11] under the assumption of a *lossless* PRS, ad are here extended to the case of a *lossy* PRS. Section II is concluded by showing that a lossy PRS can also be used for modeling a lossy dielectric cover layer.

In both Subsections II.A and II.B we will consider a *leaky* mode propagating along the z-axis of an infinite-length leaky-wave antenna (the expected effect of the aperture truncation is briefly discussed). We further assume that *i)* the structure is uniform (i.e., non-tapered), *ii)* there is a single dominant leaky mode propagating in the structure, *iii)* the structure is fed by a nondirective source so that the contribution of the element pattern can safely be neglected.

Note that the radiation efficiency considered here does not include losses due to the impedance mismatching between the feeder and the cavity, since such losses are structure-specific and have to be evaluated on a case-by-case basis. Nevertheless, an interesting work [15] has recently appeared which provides simple analytical expressions for the evaluation of losses due to impedance mismatching when canonical dipole-like sources are considered. In this regard, we should mention that [15] also provides analytic formulas for the total efficiency of LWA systems. However, those formulas apply for a different class of LWAs, for which a *sinusoidal modulation* of the PRS impedance is applied to excite a fast leaky wave [16]. These structures notably differ from the FPC-LWAs analyzed here, for which radiation occurs from the fundamental *forward* fast leaky mode excited by the application of an *nonmodulated* PRS, and thus require a different theoretical analysis.

A. Radiation Efficiency in 1-D Uniform Leaky-Wave Antennas

The analysis reported in [12] applies to traveling-wave antennas as those depicted in Fig. 1(a), i.e., 1-D unidirectional LWAs. The *leaky* modes propagating in these *partially-open* structures can be seen as perturbations of the guided modes supported by the equivalent *closed* structures, i.e., the parallel-plate waveguides (PPWs). Alternatively, leaky modes can be seen as the analytic continuation of the *surface-wave* modes propagating in the equivalent *open* structure, i.e., the grounded dielectric slab (GDS) [17], [18].

In any case, these leaky modes are characterized by generally complex wavenumbers $k_z = \beta - j\alpha$, where β is the phase constant and α is the attenuation constant (or *leakage rate*) accounting for the losses (in the case of a *lossless* structure, only those due to radiation [17]). When $\beta \gg \alpha$, the antenna radiates a scanned beam at an angle θ_0 determined solely by the normalized phase constant $\hat{\beta} = \beta/k_0 = \sin\theta_0$ [18], where k_0 is the free space wavenumber, and the hat $\hat{\cdot}$ identifies the normalization to k_0.

TABLE I
FORMULAS FOR A CORRECT EVALUATION OF THE RADIATION EFFICIENCY η_r OF LWAS OPERATING IN ANY RADIATING REGIME.

General Case ($\beta \lessgtr \alpha$)	Scanning Region ($\beta \gg \alpha$)	Broadside Region ($\beta \simeq \alpha$)
$\eta_r = \dfrac{\tan\delta_{\rm rad}}{\tan\delta_{\rm tot}} = \dfrac{\hat{\beta}_{\rm rad}\hat{\alpha}_{\rm rad}}{\hat{\beta}\hat{\alpha}}$	$\eta_r = \dfrac{\hat{\alpha}_{\rm rad}}{\hat{\alpha}}$	$\eta_r = \dfrac{\hat{\alpha}^2_{\rm rad}}{\hat{\alpha}^2_{\rm tot}}$

The scanned-beam condition $\beta \gg \alpha$ is the conventional operating regime for 1-D unidirectional LWAs, since they usually do not radiate efficiently when they operate too close to broadside or to endfire [19]. On the contrary, 1-D bidirectional LWA, as well as 2-D LWAs (such as FPC-LWAs), may produce a directive beam at broadside (see Figs. 1(b)–(c)). In particular, a broadside beam is radiated as long as $\beta < \alpha$, but the radiated power is maximized at $\beta = \alpha$ (*leaky* cutoff condition). The analysis of broadside radiation in this kind of structures has not been examined in [12]. More precisely, it was found in [12] that the radiation efficiency η_r of a traveling-wave antenna of length L is given by

$$\eta_r = \frac{\hat{\alpha}_{\rm rad}}{\hat{\alpha}}\left(1 - e^{-2\alpha L}\right), \tag{1}$$

where $\hat{\alpha}_{\rm rad}$ accounts for that portion of the *total* losses (represented by $\hat{\alpha}$) that are only due to the radiation mechanism. When the antenna is of infinite length, i.e., $L \to \infty$, the last factor vanishes and we are left with this expression:

$$\eta_r = \frac{\hat{\alpha}_{\rm rad}}{\hat{\alpha}}, \tag{2}$$

that we will consider in place of (1) without loss of generality (the efficiency of the truncated structure can always be obtained from (2) by reintroducing the last factor appearing in parentheses in (1)).

The relation in (2) is obtained through the application of the *perturbation method* [20] under the hypothesis of small losses, i.e, $\hat{\alpha} \ll 1$. However, in [12] it is further tacitly assumed that the input power remains the *same* after the introduction of radiation losses. This assumption holds as long as the modes propagating in the waveguide are considerably above cutoff (i.e., $\beta \gg \alpha$), while it can no longer be applied as the modes are approaching the *leaky* cutoff (i.e., $\beta \simeq \alpha$) and thus the structure is radiating at broadside.

In order to show this, we need a straightforward generalization of the perturbation method. Indeed, in its conventional application, the power density $P(z)$ carried along the structure is expressed as $P(z) = P(0)\exp(-2\alpha z)$, and thus the dissipation rate is $p(z) := -dP(z)/dz = 2\alpha P(z)$. In [12], the hypothesis of small losses allows for expressing the dissipation rates due to the radiation loss $p_{\rm rad}(z)$ and those due to all mechanisms of losses $p_{\rm tot}(z)$ as functions of the *same* input power $P(0)$, i.e., $p_{\rm rad}(z) = 2\alpha_{\rm rad}P(z)$ and $p_{\rm tot}(z) = 2\alpha P(z)$. When integrating these expressions with respect to z from 0 to ∞, we obtain the radiated power and the power dissipated in the structure $P_{\rm rad/tot} = \int_0^\infty p_{\rm rad/tot}(z)dz$, whose ratio gives the expression of the radiation efficiency η_r as it appears in (2). However, at the *leaky cutoff*, the leakage rate is comparable with the phase constant, and the hypothesis of small losses is no longer fulfilled. As a consequence, the dissipation rates are no longer expressible as functions of the same input power $P(0)$, but more general expressions are needed, i.e., $p_{\rm rad}(z) = 2\alpha_{\rm rad}P_{\rm rad}(z)$ and $p_{\rm tot}(z) = 2\alpha_{\rm tot}P_{\rm tot}(z)$, where $P_{\rm rad}(z) = P_{\rm rad}(0)\exp(-2\alpha_{\rm rad}z)$ and $P_{\rm tot}(z) = P_{\rm tot}(0)\exp(-2\alpha z)$, $P_{\rm rad}(0)$ and $P_{\rm tot}(0)$ representing the input powers in a *lossless* structure (i.e., where only radiation losses may occur) and a lossy structure (i.e., where all kinds of losses may occur), respectively. It then results that a more general expression for the radiation efficiency is given by

$$\eta_r = \frac{\hat{\alpha}_{\rm rad}}{\hat{\alpha}} \cdot \frac{P_{\rm rad}(0)}{P_{\rm tot}(0)}. \tag{3}$$

According to (3), in the limit of an *ideal* lossless structure, $P_{\rm rad}(0) \to P_{\rm tot}(0)$ and $\alpha_{\rm rad} \to \alpha$, leading to $\eta_r \to 1$. In order to find an expression for the ratio of the input powers $(P_{\rm rad}(0)/P_{\rm tot}(0))$, we examine the relevant case of a *lossy* PPW. In this case, the power flow in any section for either TE or TM modes is linear with $\Re\{k_z\} = \beta$ (see [20, Eqs. (3.54), (3.57)]). As an important result, the radiation efficiency of a LWA whose leaky modes are 'slight' perturbations of the TE and TM modes of an equivalent PPW-like structure is

$$\eta_r = \frac{\hat{\alpha}_{\rm rad}}{\hat{\alpha}} \cdot \frac{\hat{\beta}_{\rm rad}}{\hat{\beta}}, \tag{4}$$

where $\hat{\beta}_{\rm rad}$ is the normalized phase constant in the *lossless* structure. It is worth noting here that for a PPW-like mode propagating above cutoff, i.e., $\hat{\beta} \gg \hat{\alpha}$, $\hat{\beta}$ is not considerably affected by the introduction of losses for radiation, thus $\hat{\beta}_{\rm rad} \simeq \hat{\beta}$, and $\eta_r \simeq \hat{\alpha}_{\rm rad}/\hat{\alpha}$, recovering the original formula for the evaluation of η_r in a PPW-like structure operating in the scanning region $\hat{\beta} \gg \hat{\alpha}$ [12].

Conversely, for a PPW-like mode at cutoff we have $\hat{\beta} = \hat{\alpha}$ [11] and thus

$$\eta_r = \frac{\hat{\alpha}^2_{\rm rad}}{\hat{\alpha}^2_{\rm tot}}, \tag{5}$$

which is the sought formula for PPW-like traveling-wave antennas radiating at broadside. Remarkably, we note that the product $\hat{\beta}\hat{\alpha}$ appearing in (4) is a constant proportional to the equivalent loss tangent of a lossy PPW (see [20, eqs. (3.27)–(3.30)], [11]) and thus $\eta_r = \tan\delta_{\rm rad}/\tan\delta_{\rm tot}$. As a consequence, the radiation efficiency of a PPW-like LWA remains the same for any radiating regime (provided that the material losses are not changing within the antenna operating bandwidth). Nevertheless, the formula for its evaluation in terms of leakage rates changes. Indeed, it is important to clarify that $\hat{\alpha}_{\rm rad}$ in the broadside region differs from that in the scanning region according to its own frequency dispersion. Specifically, the former is calculated at the leaky cutoff frequency, whereas the latter is calculated at the frequency for which the desired scanning condition is reached. Nevertheless, the evaluation of η_r at broadside is more convenient, since it allows for an analytical expression of the leakage rate, as will be shown in the next Section II-B.

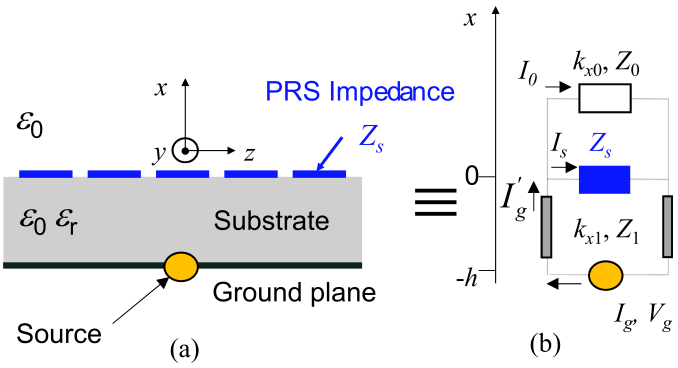

Fig. 2. 2-D section of a PRS-like FPC-LWA and its transverse equivalent network (TEN).

To summarize, Table I reports the formulas for a correct evaluation of radiation efficiency of 1-D uniform LWAs. Interestingly, these formulas still hold for the description of losses in 2-D uniform LWAs (specifically in FPC-LWAs), in spite of the different nature of the propagating leaky-wave (viz., plane leaky waves in the 1-D case, and cylindrical leaky waves in the 2-D case [21]). This result is similar to the one obtained in [11], where the analogy between 1-D bidirectional LWAs and its 2-D version is exploited to show that their radiation patterns along the principal planes are almost identical each other when radiating at broadside (in particular it was shown [11], [21] that the TE(TM) mode mainly affects radiation on the H(E)-plane, and that the TE and the TM mode look rather similar at broadside). By the same token, the contribution of losses at broadside is expected to have the same effect for 1-D bidirectional LWAs and 2-D LWAs radiating at broadside, and the results of Section III confirm this statement.

It is worth noting here that the similarity between the radiating properties of 1-D bidirectional LWAs and 2-D LWAs can also be extended to the scanning region provided that the relevant TE and TM modes excited in a 2-D LWA exhibit similar wavenumbers. However, as the scan angle increases, the wavenumbers unavoidably tend to differ from each other, in amounts that depend on the PRS properties. The validity extension to the scanning region is thus limited by the degree of equalization between the TE and the TM mode.

As a final remark, we should also note that 2-D LWAs can also be designed to support a single TE/TM mode, thus not being able to radiate a broadside beam, but an omnidirectional conical beam [21]. In this case, the radiation pattern of a 2-D LWA at an arbitrary azimuthal cut is the same of an *equivalent* 1-D bidirectional LWA (i.e., modeled with the same PRS), thus results of Table I extends to this class of antennas without requiring any additional hypothesis.

B. 2-D Uniform Fabry-Perot Cavity Leaky-Wave Antennas

In the previous Subsection II-A we have derived expressions for evaluating the radiation efficiency of uniform LWAs radiating at broadside. A significant class of 2-D uniform LWAs that efficiently radiate a directive beam at broadside are FPC-LWAs [9], [11]. This type of structures consists of a GDS covered with a PRS as sketched in Fig. 1(c). The simple transverse equivalent network (TEN) in Fig. 2 has been proven to accurately model FPC-LWAs where the PRS is either a homogenized nonmodulated metasurface or a superstrate dielectric layer [14]. The application of the transverse resonance technique to the TEN model, allows for deriving the dispersion equation of such FPC-LWAs. From the analysis of the dispersion equation, the fundamental properties of broadside radiation from FPC-LWAs have rigorously been obtained in [11]. However, the analysis in [11] assume a *lossless PRS*, i.e., characterized by a purely imaginary sheet admittance $Y_s = jB_s$, with B_s the sheet susceptance. This assumption is rather restrictive for a rigorous investigation of FPC-LWAs in the THz range, where the PRS might exhibit non-negligible losses.

When a lossy PRS is considered, the dispersion equation of an FPC-LWA radiating at broadside takes the following form:

$$\bar{Y}_0 + \bar{Y}_s - j\bar{Y}_1 \cot(k_0 h \hat{k}_{x1}) = 0, \tag{6}$$

where the bar $\bar{\cdot}$ identifies normalization to the free-space impedance $\eta_0 \simeq 120\pi\,\Omega$, $\bar{Y}_s = \bar{G}_s + j\bar{B}_s$ is the generally lossy normalized sheet admittance of the PRS ($\bar{G}_s$ and $\bar{B}_s$ being the normalized conductance and susceptance), $\bar{Y}_0$, $\bar{Y}_1$ are the normalized characteristic admittances in air and inside the slab, respectively, $\hat{k}_{x1} = \sqrt{\mu_r \varepsilon_r - \hat{k}_z^2}$ is the normalized transverse (vertical) wavenumber inside the slab of thickness h, relative permeability μ_r and permittivity $\varepsilon_r = \varepsilon_r' - j\tan\delta_\varepsilon$, where $\tan\delta_\varepsilon$ is the loss tangent accounting for the dielectric losses of the substrate, and $\varepsilon_r' = \Re\{\varepsilon_r\}$.

Under the hypothesis of broadside radiation, i.e, $\hat{k}_z = (1-j)\hat{\alpha}_z$, small dielectric losses, i.e., $\tan\delta_\varepsilon \ll 1$, and large $\bar{B}_s$, i.e., $\bar{B}_s \gg 1$ (as typically required to obtain a directive beam), we do not need to distinguish between the TE and TM polarization case, since the normalized characteristic admittances can be approximated with the expressions $\bar{Y}_0 \simeq 1$ and $\bar{Y}_0 \simeq \sqrt{\varepsilon_r'/\mu_r}$ for both polarizations. As discussed in [11], by equating the imaginary parts of (6) to 0, a design rule for the slab thickness is found, which reads $h \simeq 0.5 m\lambda/\sqrt{\mu_r \varepsilon_r'}$, where $m \in \mathbb{Z}^+$ is the modal index that identifies the order of the leaky-mode pair excited in the cavity. Therefore, for the fundamental pair of TE/TM leaky modes, i.e., $m = 1$, (6) can be recast in the form:

$$\sqrt{\frac{\mu_r}{\varepsilon_r'}} \tan\left(\pi \sqrt{1 - j\tan\delta_\varepsilon + j\frac{2\alpha^2}{\mu_r \varepsilon_r'}}\right) = \frac{j}{1 + \bar{G}_s + j\bar{B}_s}. \tag{7}$$

From (7), using the Taylor approximation for the tangent function, an expression for $\hat{\alpha}_z$ is found after simple algebraic manipulations

$$\hat{\alpha} \simeq \sqrt{\frac{\mu_r \varepsilon_r'}{\pi}\sqrt{\frac{\varepsilon_r'}{\mu_r}}\frac{1+\bar{G}_s}{(1+\bar{G}_s)^2 + \bar{B}_s^2} + \frac{\tan\delta_\varepsilon \mu_r \varepsilon_r'}{2}}, \tag{8}$$

where the second term under the square root is the same one appearing in [11, eq. (21)] and accounting for the substrate losses. A further comparison with [11, eq. (21)] suggests to rearrange the terms appearing in (8) so as to express $\hat{\alpha}_z$ as follows:

$$\hat{\alpha} = \sqrt{\hat{\alpha}_{\text{rad}}^2 + \hat{\alpha}_{\text{PRS}}^2 + \hat{\alpha}_{\text{sub}}^2}, \tag{9}$$

where, with the obvious meaning of subscripts,

$$\hat{\alpha}_{\rm rad} = \sqrt{\frac{\sqrt{\mu_r\varepsilon_r'}^3}{\mu_r\pi}\frac{1}{1+\bar{B}_s^2}} \simeq \frac{\varepsilon_r'^{3/4}}{\sqrt{\pi}\bar{B}_s}, \tag{10}$$

$$\hat{\alpha}_{\rm PRS} = \sqrt{\frac{\sqrt{\mu_r\varepsilon_r'}^3}{\mu_r\pi}\frac{\bar{G}_s}{(1+\bar{B}_s^2)}\frac{(\bar{B}_s^2-1-\bar{G}_s)}{(1+\bar{G}_s)^2+\bar{B}_s^2}} \simeq \frac{\varepsilon_r'^{3/4}}{\sqrt{\pi}}\frac{\sqrt{\bar{G}_s}}{\bar{B}_s}, \tag{11}$$

$$\hat{\alpha}_{\rm sub} = \sqrt{\frac{\tan\delta_\varepsilon\mu_r\varepsilon_r'}{2}} \simeq \sqrt{\frac{\tan\delta_\varepsilon\varepsilon_r'}{2}}, \tag{12}$$

where the last approximations hold for $\mu_r \simeq 1$ and large $\bar{B}_s$. The proposed representation is rather convenient because it allows for recognizing the term $\hat{\alpha}_{\rm PRS}$ as an independent contribution that account for the losses due to the PRS. This is an important result, since it extends the previous analysis for lossless PRS, that is now included in the limit case for $\bar{G}_s = 0$.

Moreover, the results of (9)–(12) allow for distinguishing the different ways in which the input power is dissipated by the FPC-LWA. In particular, according to the results of the previous Subsection II-A, it is possible to define the following figures of merit:

$$\eta_r := \alpha_{\rm rad}^2/\alpha^2, \tag{13}$$

$$r_{\rm PRS} := \alpha_{\rm PRS}^2/\alpha^2, \tag{14}$$

$$r_{\rm sub} := \alpha_{\rm sub}^2/\alpha^2, \tag{15}$$

which represent the radiation efficiency η_r, the PRS loss ratio $r_{\rm PRS}$, and the substrate loss ratio $r_{\rm sub}$. With these definitions at hand, it is interesting to examine the case $\tan\delta_\varepsilon = 0$, since in this case, the radiation efficiency clearly does not depend on ε_r. More precisely, it results that the radiation efficiency reads:

$$\eta_r = \frac{1}{1+\bar{G}_s} + \frac{\bar{G}_s}{1+\bar{B}_s^2} + \frac{\bar{G}_s}{(1+\bar{G}_s)(1+\bar{B}_s^2)} \simeq \frac{1}{1+\bar{G}_s}, \tag{16}$$

where the last approximation holds in the asymptotic limit $\bar{B}_s \gg 1$. Interestingly, the last asymptotic result can also be obtained through a simple circuit analysis of the TEN in Fig. 2. Indeed, the radiation efficiency is equivalently defined as the ratio between the real parts of the power radiated into free space and the total power $\eta_r = \Re\{P_{\rm rad}\}/\Re\{P_s+P_{\rm rad}\}$, where $P_{\rm rad} = |I_0|^2/2Y_0$ and $P_s = |I_s|^2/2Y_s$, hence $\eta_r = 1/(1+\bar{G}_s)$ (in the last step we exploited that $|I_s|/|I_0| = |Y_s|/|Y_0|$, and that $\bar{G}_0 = \Re\{\bar{Y}_0\} \simeq 1$ at broadside for large $\bar{B}_s$).

Finally, it is interesting to note that (9)–(12), seen as a generalization of [11, eq. (21)], allow for an estimation of the hyperbolic locus of the leaky wavenumber in the complex $\hat{k}_z$-plane that characterizes any PRS-based FPC-LWA and reads

$$\hat{\beta}\hat{\alpha} = \frac{\mu_r\varepsilon_r'}{2}\tan\delta_{\rm eq} = C, \tag{17}$$

where C is a constant, whereas the equivalent loss tangent $\tan\delta_{\rm eq}$ models both radiation and material losses of the structure. Indeed, since leaky modes in a PRS-based FPC-LWA must obey this condition at any frequency, it must be true even at broadside where we know $\hat{\beta} \simeq \hat{\alpha}$, thus $C = \hat{\alpha}^2$, and through (8)

$$C = \frac{\mu_r\varepsilon_r'}{2}\left[\tan\delta_\varepsilon + \sqrt{\frac{\varepsilon_r'}{\mu_r}}\frac{2}{\pi}\frac{1+\bar{G}_s}{(1+\bar{G}_s)^2+\bar{B}_s^2}\right], \tag{18}$$

we get the sought closed-form expression for the hyperbolic wavenumber locus of a lossy PRS-based FPC-LWA. Following the same formalism of (10)–(12), we can express the equivalent loss tangent as the sum of three terms

$$\tan\delta_{\rm eq} = \tan\delta_\varepsilon + \tan\delta_{\rm rad} + \tan\delta_{\rm PRS}, \tag{19}$$

where

$$\tan\delta_{\rm rad} = \frac{2}{\pi}\sqrt{\frac{\varepsilon_r'}{\mu_r}}\frac{1}{1+\bar{B}_s^2}, \tag{20}$$

$$\tan\delta_{\rm PRS} = \frac{2}{\pi}\sqrt{\frac{\varepsilon_r'}{\mu_r}}\frac{\bar{G}_s}{(1+\bar{B}_s^2)}\frac{(\bar{B}_s^2-1-\bar{G}_s)}{(1+\bar{G}_s)^2+\bar{B}_s^2}, \tag{21}$$

and thus the ratios between each term appearing in the right-hand side of (19) and $\tan\delta_{\rm eq}$ can equivalently be used to recover the definitions in (13)–(15), also in agreement with the results of the previous Subsection II-A (see Table I).

The formulas obtained so far apply for FPC-LWAs based on lossy PRS. We conclude this Section II by showing that a lossy PRS may also be used to model a dielectric cover layer, thus extending the range of applicability of the previous formulas to a different kind of FPC-LWAs, namely substrate-superstrate LWAs (SS-LWAs) [22], [23].

As shown in [14], SS-LWAs can be studied as PRS-like FPC-LWAs, by modeling the superstrate layer with an equivalent PRS. At a first glance, this equivalence would allow for studying the radiation efficiency of the SS-LWA by applying the formulas (8)–(13) to the equivalent PRS model. However, the analysis in [14] only applies to *lossless* superstrates, a hypothesis that is no longer satisfied by directive SS-LWAs designed, e.g., in the THz range. Indeed, the directivity of a SS-LWA is closely related to the 'step-index' (i.e., the ratio between the refractive indices of the superstrate and the substrate), thus a directive SS-LWA would require a high-permittivity material, which usually exhibits considerable dielectric losses.

However, the equivalent model proposed in [14] can be extended to the relevant case of *lossy* superstrates. In particular, it is found that (see Appendix), to a first order of approximation, a lossy superstrate can accurately be modeled by a lossy PRS with an equivalent complex-valued normalized admittance $\bar{Y}_s$ given by:

$$\bar{Y}_s = \sqrt{\varepsilon_{r2}'}\left(\frac{\pi}{2}\sin\frac{\delta_{\varepsilon 2}}{2} + j\right), \tag{22}$$

where $\varepsilon_{r2} = \varepsilon_{r2}'(1 - j\tan\delta_{\varepsilon 2})$ is the complex permittivity of the superstrate. This expression will be proven to be remarkably accurate for highly-reflective superstrate in Subsection IV-B. The following Section III is instead devoted to the analysis of PRS-like FPC-LWAs only.

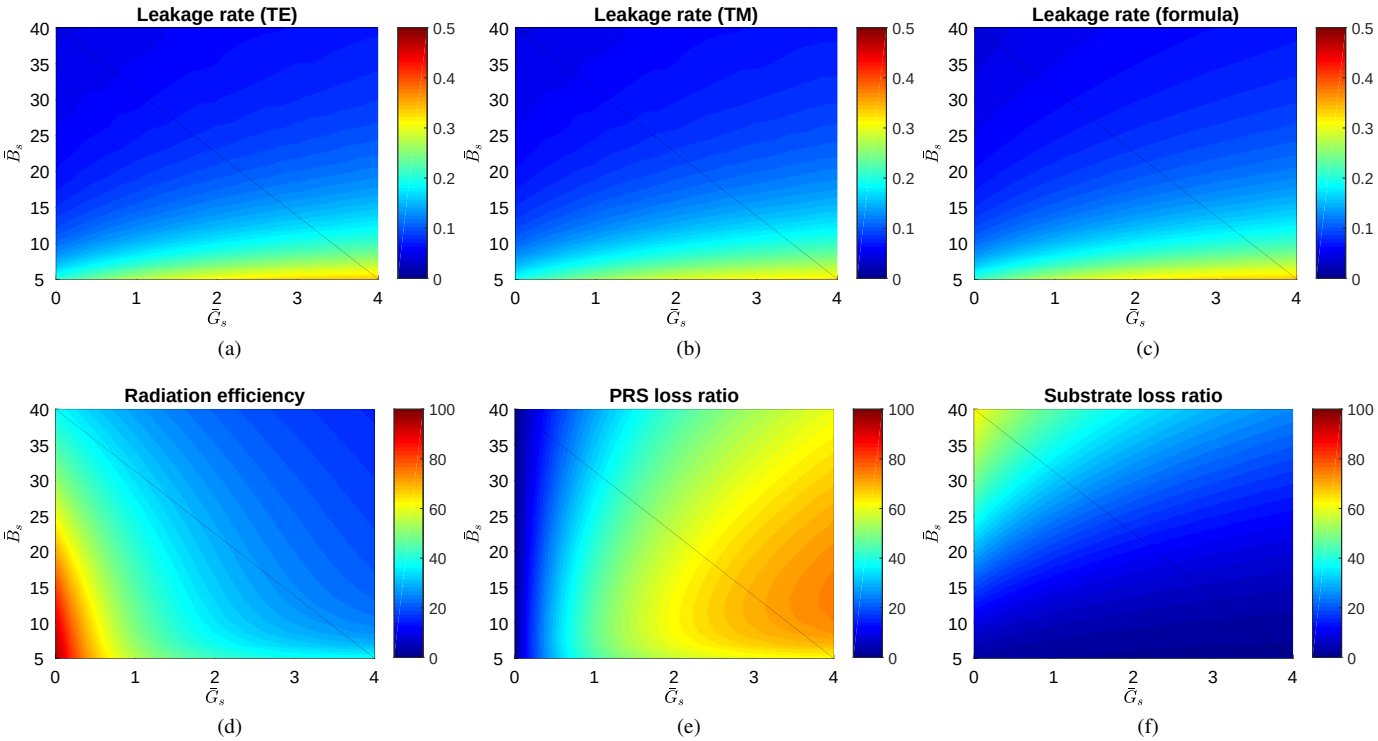

Fig. 3. (a)–(c) Colormaps of the leakage rate $\hat{\alpha}$ evaluated at the leaky cutoff frequency f_c and represented as a two-dimensional function of the normalized conductance $\bar{G}_s$ (in the range $0-4$) and the normalized susceptance $\bar{B}_s$ (in the range $5-40$). In (a) and (b) the numerical results for the TE and the TM case, respectively, whereas in (c) the analytic results given by (8). In all results a substrate with a complex permittivity $\varepsilon_r = 2.3(1-j0.001)$ is assumed. (d)–(f) Analytic results showing (d) the radiation efficiency (using (13) with (10)), (e) the losses in the PRS (using (14) with (11)), and (e) the losses in the substrate (using (15) with (12)), as functions of $\bar{G}_s$ and $\bar{B}_s$ in the same ranges of (a)–(c).

III. Results

The results of the previous Subsections II-A and II-B furnished simple analytical expressions, namely (13)–(15) with (9)–(12), for evaluating the radiation efficiency and the losses in PRS-like FPC-LWAs. To validate these expressions we report here both numerical and full-wave simulations. In Subsection III-A we first show that the closed-form expressions derived in (9)–(12) for the leakage rates agree well with the results obtained through an accurate numerical solution of the dispersion equation in (6) for different values of $\bar{G}_s$ and $\bar{B}_s$. Once we have assessed the accuracy of (9)–(12), we show in Subsection III-B that the formulas for the radiation efficiency (13) and that for the losses (14)–(15) agree well with the results obtained from full-wave simulations of PRS-based FPC-LWAs for different values of the sheet impedance and the loss tangent. The full-wave validation not only confirms the accuracy of the proposed formulas, but also corroborate the consistency of a leaky-wave analysis of this class of structures.

A. Numerical Results

The complex roots of the dispersion equation in (6) are the eigenvalues of the modes supported by the structure. Since we are interested in forward fast leaky modes, we consider only solutions for which $0 \leq \beta \leq k_0$, and $\Im\{\hat{k}_{x0}\} > 0$ (as required by the improper character of such waves [17], [18]), where $\hat{k}_{x0} = \sqrt{1-\hat{k}_z^2}$. We have therefore applied the Padé algorithm [24] (a root-finding algorithm particularly suitable for searching complex modes in FPC-LWAs) to (6) for different values of $\bar{G}_s$ and $\bar{B}_s$ to solve for both the TE and TM leaky modes, thus obtaining the corresponding dispersion curves. Since we are mainly interested in the value of the leakage rates at the leaky cutoff (viz., the frequency f_c for which $\beta(f_c) \simeq \alpha(f_c)$), we have not reported the whole dispersion curves, but just the values $\hat{\alpha}$ at f_c for both the TE and the TM case (see Fig. 3(a) and Fig. 3(b), respectively) and compared them with the values obtained through the application of (8) (see Fig. 3(c)).

The analysis in Figs. 3(a)–(f) is carried out for $0 < \bar{G}_s < 4$ and $5 < \bar{B}_s < 40$, assuming a substrate material (Teflon) of thickness $h = 0.5\lambda\sqrt{\varepsilon_r'}$ with $\varepsilon_r' = 2.3$ and loss tangent of $\tan\delta_\varepsilon = 0.001$. We should mention that the effect of the loss tangent on the radiation efficiency will be discussed in the following Subsection III-B, whereas the effect of ε_r' can be easily predicted from (19)–(21) and is thus not shown. In particular, it is clear from (19)–(21) that η_r and r_{PRS} increase as ε_r' increases, whereas r_{sub} decreases. However, for most of materials, as ε_r' increases the loss tangent increases as well, hence the benefits in using high-permittivity materials are partially washed out by the higher loss tangents.

We should also discuss the choice of the ranges $0 < \bar{G}_s < 4$ and $5 < \bar{B}_s < 40$ for the lossy PRS. As can be inferred from (16), for $0 < \bar{G}_s < 4$, the radiation efficiencies would span the range $20\% < \eta_r < 100\%$ (neglecting substrate losses) which covers almost any practical antenna design. With regard to the lower bound of the $\bar{B}_s$ range, it should be noticed that (11)

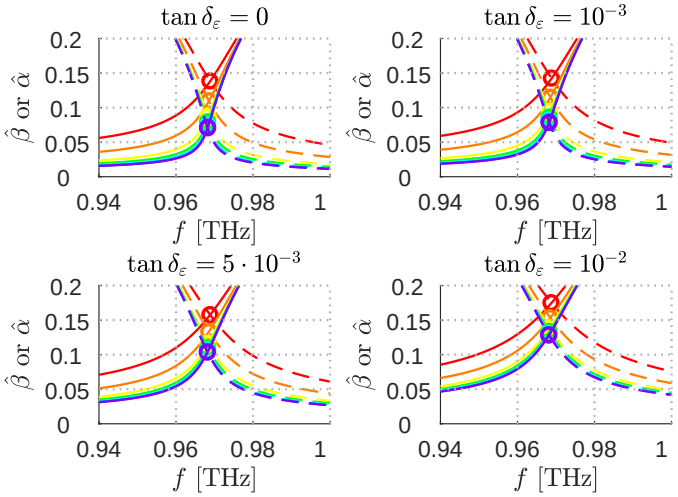

Fig. 4. Dispersion curves $\hat{\beta}$ and $\hat{\alpha}$ vs. frequency in colored solid and dashed lines respectively, for four different values of loss tangents ($\tan\delta_\varepsilon = 0,\ 0.001,\ 0.005,\ 0.01$ going clockwise from the upper-left corner) and seven different values of sheet resistance ($R_s = 0,\ 0.1,\ 0.25,\ 0.5,\ 1,\ 2.5,\ 5\,\Omega$ in violet, blue, cyan, green, yellow, orange, and red, respectively), for a fixed sheet reactance $X_s = 25\,\Omega$. The frequency dispersion is reported in the range $0.94 \le f \le 1$ THz close to the leaky cutoff (highlighted with a colored circle for each corresponding colored curve). Note that the violet ($R_s = 0\,\Omega$) and blue ($R_s = 0.1\,\Omega$) lines overlap each other and are thus not distinguishable.

is well defined only for $\bar{B}_s > \sqrt{1+\bar{G}_s}$. Hence for $\bar{G}_s = 4$, $\bar{B}_s > \sqrt{5}$, thus $\bar{B}_s > 5$ represents a conservative choice. With regard to the upper bound of the $\bar{B}_s$ range, it should be noticed that for $\varepsilon_r' = 2.3$ and $\bar{B}_s = 40$, (10) gives $\hat{\alpha}_{\rm rad} \simeq 0.026$, that, for a lossless PRS-like FPC-LWA, would correspond to a broadside beam with a half-power beamwidth of $\Delta\theta \simeq 4^\circ$ (using the well-known formula $\Delta\theta = 2\sqrt{2}\hat{\alpha}$ [3]), which is rather directive ($D_0 \simeq 4\pi/\Delta\theta^2 \simeq 33\,\mathrm{dB}$).

We can now comment the results of Figs. 3(a)–(c). As expected, the difference between the TE and the TM case is negligible except for considerably small values of $\bar{B}_s$, namely $\bar{B}_s \to 5$, where, however, the structure is no longer capable of producing a directive beam, since the condition $\bar{B}_s \gg 1$ is no longer fulfilled. Over the whole range, a remarkable agreement is observed leading to an average percent error around 0.5% (almost comparable with the numerical error of the root-finding algorithm), with an isolated narrow peak of error for $\bar{B}_s,\ \bar{G}_s \to 4$, where the maximum error, however, is around 5%.

To complete the picture, in Figs. 3(d)–(f), equations (13)–(15) with (9)–(12) have been evaluated under the same conditions of Figs. 3(a)–(c). As shown, the radiation efficiency decreases abruptly for $\bar{G}_s > 2$ for any value of $\bar{B}_s$. Since we have chosen a loss tangent $\tan\delta_\varepsilon = 0.001$, most of the power is dissipated into the lossy PRS rather than in the lossy substrate, except for highly-reflective (high $\bar{B}_s$) and almost lossless (low $\bar{G}_s$) PRS, for which the substrate losses are not negligible. This effect could easily be predicted from (19)–(21), from which it is readily obtained that for $\varepsilon_r' = 2.3$, $\bar{G}_s \to 0$, and $\bar{B}_s \simeq 40$, it results $\tan\delta_{\rm PRS} \to 0$, whereas $\tan\delta_{\rm rad} \simeq \tan\delta_{\rm sub}$, thus motivating a radiation efficiency slightly greater than 50% (see the upper-left corner of Fig. 3(d)). A more comprehensive analysis is reported in the next Subsection III-B, where numerical and full-wave validations are performed for different values of loss tangents and sheet resistances $R_s = \Re\{Z_s\}$, $Z_s = Y_s^{-1} = R_s + jX_s$ being the sheet impedance, and $X_s = \Im\{Z_s\}$ is the sheet reactance.

B. Full-Wave Results

In this Subsection we validate the leaky-wave analysis of an FPC-LWA based on a lossy PRS through a set of full-wave simulations performed with the commercial solver CST Microwave Studio [25]. This solver allows for enforcing an impedance boundary condition characterized by a complex scalar value $Z_s = R_s + jX_s$ that accurately models a lossy PRS. (We note here that in this Subsection, we switched from the 'admittance formalism', which is rather convenient for the analysis of the TEN, to the 'impedance formalism' that is used in CST).

We have therefore simulated several PRS-like FPC-LWAs designed at the frequency of 1 THz and consisting of a GDS with $\varepsilon_r' = 2.3$ and $\tan\delta_\varepsilon = 0, 1, 0.001, 1, 0.005, 1, 0.01$ covered with a lossy PRS with $X_s = 25\ \Omega$ and $R_s = 0,\ 0.1,\ 0.25,\ 0.5,\ 1,\ 2.5,\ 5\ \Omega$, and then evaluated the radiation efficiency at the theoretical leaky cutoff f_c. The simulated structure has a lateral truncation at $L = 20\lambda$, such that the fraction of power that is neither radiated nor dissipated in the materials is less than 0.0001 for the lossless case (for the lossy cases will be much less). Therefore, the effect of the aperture truncation can safely be neglected from the following analysis of efficiencies. The horizontal dipole-like source that is needed to excite both the fundamental TE and TM leaky modes is modeled by a quasi-resonant slot etched in the ground plane and fed through a THz waveguide transition [26] (some details are provided in [9]).

In all cases the far-field patterns have been evaluated with CST (results have not been reported) to verify that the antenna was actually radiating a broadside beam at f_c, as predicted by the leaky-wave analysis. The cutoff frequency f_c has been found numerically, by examining the dispersion curves reported in Fig. 4. In all cases $f_c \simeq 0.968$ THz, a value that could also be predicted with a good accuracy by the analytical expressions reported in [9], [11] for FPC-LWAs based on lossless PRSs. It is worth noting that, for frequencies below cutoff, $\hat{\alpha}$ has to increase to compensate for the decrease of $\hat{\beta}$, as dictated by (17). This behavior is common to all mechanisms of losses, and reflects the reactive nature of the fields below cutoff. Accordingly, the directivity (which is inversely proportional to $\hat{\alpha}^2$) abruptly decreases below cutoff, being the fields mostly reactive rather than radiative.

As shown in Fig. 4, the agreement between the numerical results (look at the crossing point between the dashed and solid lines) and the analytical formula (8) (the circles) is remarkably good in all cases. The value of the leakage rate at the cutoff frequency in the lossless case, i.e., $R_s = 0\ \Omega$ and $\tan\delta_\varepsilon = 0$ (see the intersection of the violet curves at the upper-left corner of 4), provides for a numerical evaluation of $\alpha_{\rm rad}$, thus allowing for computing the radiation efficiency in all cases according to (13).

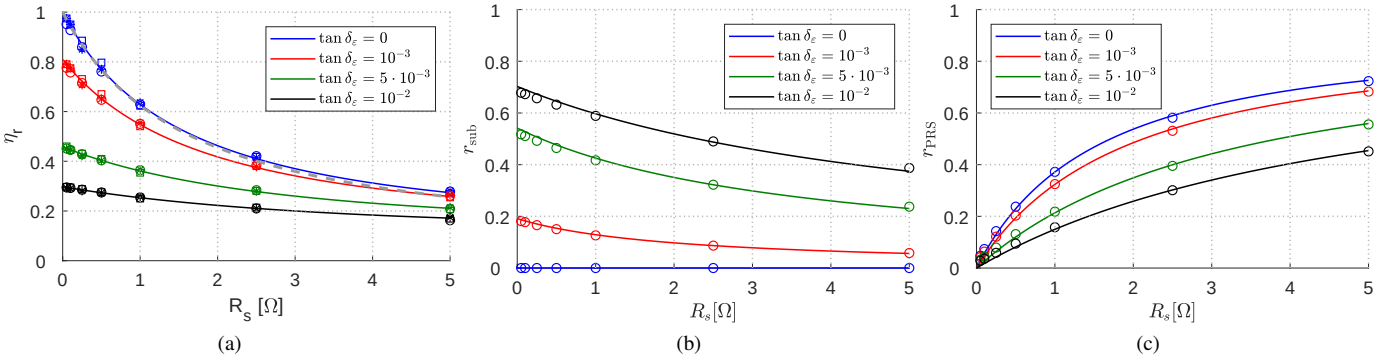

(a) (b) (c)

Fig. 5. (a)–(c) Comparison between analytic results (solid lines) and full-wave simulations (circles) for (a) the radiation efficiency, (b) the losses in the substrate, and (c) the losses in the PRS, as functions of the sheet resistance R_s for different values of the loss tangent ($\tan\delta_\varepsilon = 0,\ 0.001,\ 0.005,\ 0.01$ in blue, red, green, and black, respectively). In (a), numerical results for the TE and the TM cases are also reported in colored squares and colored asterisks, respectively, whereas the dashed gray line represents the asymptotic expression (16) for the lossless substrate. Other parameters: $X_s = 25\,\Omega$, $\varepsilon_r' = 2.3$.

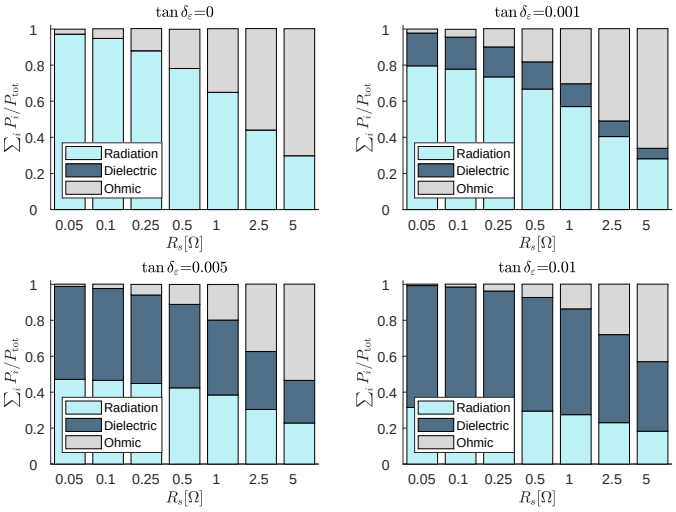

Fig. 6. A bar plot, showing how the power is distributed in different ways, i.e., radiation, dielectric, and ohmic losses. Their sum is always one, since they represent the only existing mechanisms of power dissipation of the structure.

In this regard, the numerical evaluation of the radiation efficiency has been reported in Fig. 5(a) (colored squares and asterisks for the TE and the TM case, respectively) and compared with both the full-wave results (colored circles) and the analytic expression (colored solid lines). The agreement between all kinds of evaluations is impressive and confirms the consistency of the methods proposed in this work. As expected, for the lossless case the radiation efficiency is 100%, and monotonically decreases as R_s and $\tan\delta_\varepsilon$ increase. Interestingly, when a lossless substrate is considered, even the agreement with (16) (reported with a gray dashed line in Fig. 5(a)) is remarkably good.

To complete the full-wave validation of (13)–(15) with (9)–(12), the losses in the material and in the PRS have been reported in Figs. 5(b)–(c), for the same case study of Fig. 5(a). As shown, the agreement between the formulas and the full-wave results is again excellent. A similar agreement was obtained for different values of X_s (specifically, a few cases with $X_s = 15,\ 50\,\Omega$ have been validated), and not reported for the sake of conciseness.

To conclude the analysis reported in this Subsection III-B, in Fig. 6 we show a bar graph to give a more immediate view of how the input power is distributing in the structure, for the case study previously analyzed. From Fig. 6, one has a clear picture on the radiating performance of this class of devices, as the losses in both the PRS and the substrate change. In particular, we note that a sheet resistance of $R_s = 5\ \Omega$ leads to very low radiation efficiencies (always less than 30%) even when a lossless substrate is employed. However, we should note that the quantitative impact of the loss tangent and the sheet resistance are dictated by the choice of the sheet reactance and of the real part of the permittivity, which have been here fixed to $X_s = 25\ \Omega$, and to $\varepsilon_r' = 2.3$, respectively. The effect of a different choice of ε_r' has been commented before; as concerns the effects related to a different choice of X_s, for a lower (higher) value of X_s the loss tangent and the sheet resistance would have a higher (lower) impact on the radiation efficiency.

IV. Antenna Applications

In this Section IV, we aim at showing how the results derived and validated in the previous Sections II–III can turn extremely useful in various cases of practical interest in the context of antenna applications, spanning from microwave to THz frequencies. Indeed, even in this high frequency range, various kinds of FPC-LWAs have recently been proposed [10]. Here, we discuss three relevant cases: two THz antennas, namely a graphene-based FPC-LWA (Subsection IV-A) and a substrate-superstrate FPC-LWA (Subsection IV-B), and a microwave FPC-LWA based on a commercial lossy laminate. For all cases, the far-field radiation patterns and the radiation efficiencies are evaluated with both analytical means and full-wave simulations.

A. Graphene FPC-LWAs

Graphene, the two-dimensional version of graphite, is an attractive material for THz antenna applications [27] since in this frequency range it shows moderate ohmic losses and, more importantly, its impedance can be switched from low to high values, thus allowing for pattern reconfigurability at

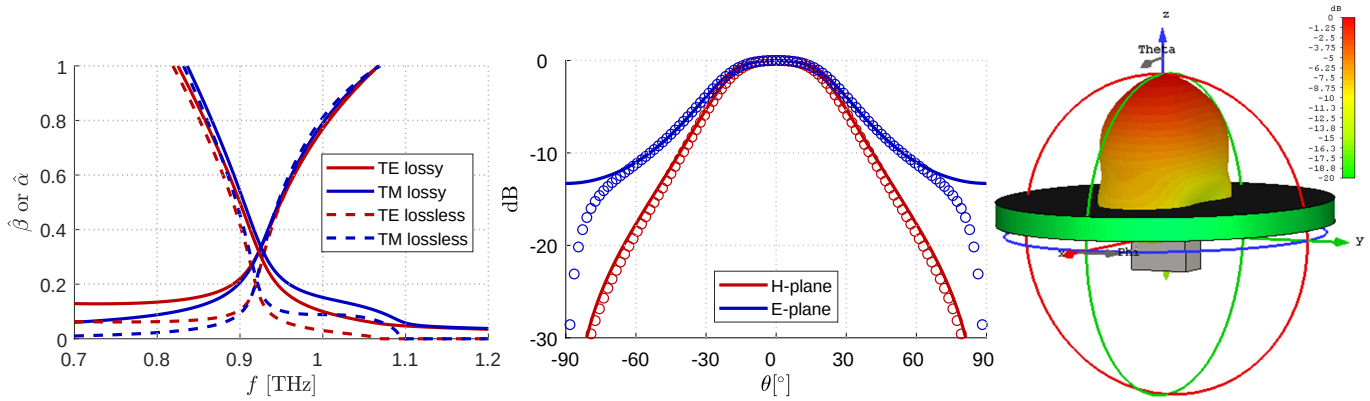

(a) (b) (c)

Fig. 7. Results for the case study of Subsection IV.A (Graphene FPC-LWAs). (a) Dispersion curves $\hat{\beta}$ and $\hat{\alpha}$ vs. frequency for the TE and TM modes (in red and blue lines, respectively) in the lossy case (solid lines) and the lossless case (dashed lines). (b) Normalized radiation patterns over the H-plane (in red) and E-plane (in blue) of the lossy structure, considering asymptotic leaky patterns (solid lines) and the total pattern (circles). (c) 3-D Radiation pattern obtained through a full-wave simulation of the truncated structure.

fixed frequency [8]. From a modeling point of view, another important feature is that, in the low THz range, i.e., for $0.3 \leq f \leq 3$ [THz], and at room temperature, i.e., $T = 300$ K, graphene can be treated as a lossy PRS, whose expression is sufficiently well-described in analytical closed-form, by retaining only the intraband contribution of Kubo formula [28], which reads

$$Y_{\rm g} = S(\mu_c, T)\left(\frac{\tau}{1+(\omega\tau)^2} + j\frac{\omega\tau^2}{1+(\omega\tau)^2}\right), \qquad (23)$$
$$S(\mu_c, T) = \frac{2q_e K_B T}{\pi\hbar^2}\ln\left[2\cosh\left(\frac{\mu_{\rm c}}{K_B T}\right)\right],$$

where $\omega = 2\pi f$ is the angular frequency, q_e is the electron charge, k_B is the Boltzmann constant, $\hbar$ is the reduced Planck constant, $\mu_{\rm c}$ is the chemical potential, and τ the relaxation time. As shown in [8], $Y_{\rm g}$ becomes mostly reactive for high values of μ_c and τ, so in the following we fix $\mu_{\rm c} = 1$ eV and $\tau = 1$ ps. Both values are within the state-of-the art of synthesis methods [8], [29], provided that the graphene sheet is deposited on a suitable dielectric substrate, which motivates the choice of a quartz substrate ($\varepsilon_r = 3.842$, $\tan\delta_\varepsilon = 0.007$ at $f = 1$ THz [30]) of thickness $h = 0.5\lambda_0/\sqrt{\varepsilon_r'} \simeq 77\,\mu$m. Under these conditions, for $f = 1$ THz, a graphene sheet shows a complex-valued normalized admittance of $\bar{Y}_{\rm g} := Y_{\rm g}\eta_0 = 1.282 - j7.431$. We should note that these values barely fulfill the hypothesis of high reflectivity and small losses, i.e., $\Im\{\bar{Y}_{\rm g}\} \gg 1$ and $|\Re\{\bar{Y}_{\rm g}\}| \ll 1$, required for obtaining accurate results from the application of the leaky-wave analysis. Nevertheless, equations (8) and (13), even if obtained under the frame of the leaky-wave analysis, still provide remarkably and unexpectedly accurate results, as is readily shown.

Specifically, with these values of $Y_{\rm g}$ at hand, the application of (8) and (13) predicts a leakage rate $\hat{\alpha} \simeq 0.32$, and a radiation efficiency $\eta_r \simeq 41\%$. Both results are confirmed by the numerical dispersion analysis reported in Fig. 7(a), where the dispersion curves for the lossy structure are reported in solid lines, and compared with those obtained for the lossless structure (i.e., considering only the real parts of the dielectric permittivity and the graphene conductivity). It is worth noting here that the difference between the values of $\hat{\beta}$ in the lossy and the lossless case is no longer appreciable as we move away from the leaky cutoff, thus confirming the validity of the approximation made in [12]. Conversely, close to the leaky cutoff, the value of $\hat{\beta}$ in the lossy case considerably differs from that obtained in the lossless case, thus motivating the analysis of Section II and the results of Table I.

TABLE II
COMPARISON BETWEEN ANALYTICAL, NUMERICAL, AND FULL-WAVE RESULTS FOR THE RADIATION EFFICIENCY OF THE CASE STUDIES REPORTED IN SECTION IV.

Case study	Analytical	Numerical TE(TM)	Full-wave
Graphene	41%	40.3%(39.2%)	39.7%
Substrate-Superstrate	N/A	61.02%(62.02%)	61.8%
Equivalent PRS model	61.8%	61.5%(60.4%)	62.8%
PRS-based	47.7%	45.9%(46.0%)	46.9%

To give a more comprehensive overview of the radiation problem, the normalized power patterns over the principal planes (i.e., the E and H planes which are determined by the TE and TM leaky modes, respectively) have been calculated using the asymptotic formulas for the *leaky* patterns of FPC-LWAs (see, e.g., [11, Eq. (4)]) and reported in Fig. 7(b) (see solid lines), where they have been compared with the results obtained through the application of the reciprocity theorem (see colored circles). The good agreement between the results confirm that, despite the relatively high value of the leakage rate (in [18] it was shown that *leaky* patterns are expected to be a good representation of the *total* pattern, which also accounts for the spatial-wave contribution, for $\hat{\alpha} < 0.2$), the leaky modes are still the dominant contribution to the radiation pattern. A full-wave simulation of the structure further corroborates this result, as can be inferred from the 3-D radiation pattern shown in Fig. 7(c). Finally, in Table II, analytical

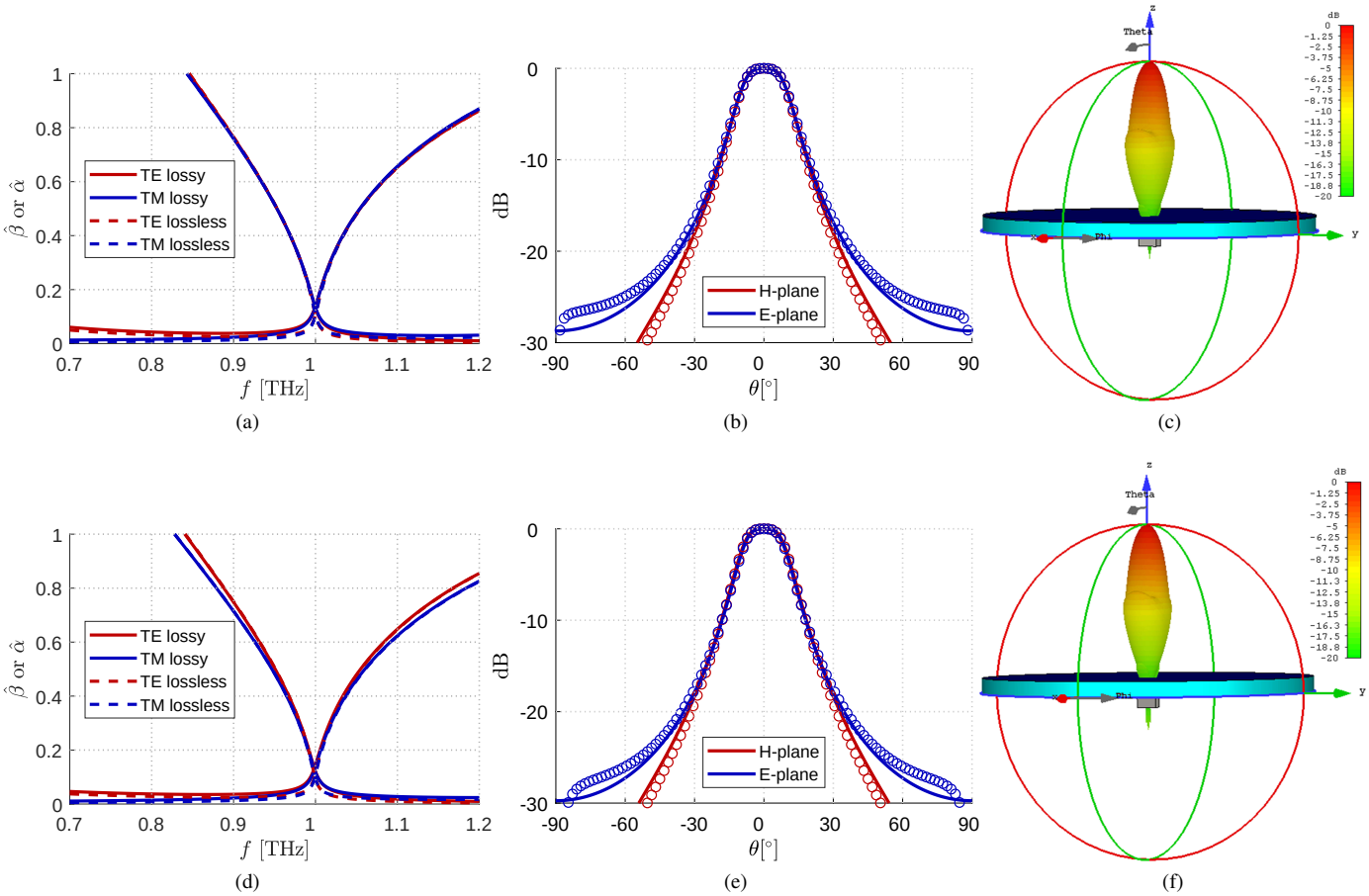

Fig. 8. Results for the case study of Subsection IV.B (Substrate-superstrate LWAs). (a)–(c) As in Figs. 7(a)–(c), but for the SS-LWA. (d)–(f) As above, but for the equivalent PRS model of the SS-LWA. Both numerical and full-wave results confirm the equivalence between the SS-LWA and its PRS model.

numerical, and full-wave results for the radiation efficiency of this case study (first row of Table II) are compared, to better appreciate the accuracy of the proposed formulas.

B. Substrate-superstrate LWAs

Substrate-superstrate planar antennas were originally proposed in [22], and only later the role of the leaky waves were recognized to provide for a convenient explanation of the radiation mechanism [23] in such planar structures. Since then, they are commonly referred as Substrate-Superstrate (SS) LWAs, and they are currently being proposed in THz and optical antenna applications, where the use of metals has to be reduced as much as possible to mitigate the impact of ohmic losses.

We consider here a SS-LWA designed at $f = 1$ THz and consisting of a low-loss dielectric material as substrate, and a very high-permittivity dielectric material as superstrate, namely, Zeonor ($\varepsilon_{r1} = 2.3(1-j0.002)$ at $f = 1$ THz [31]) and Zirconium Tin Titanate II ($\varepsilon_{r2} \simeq 98(1-j0.055)$ at $f = 1$ THz [32]), respectively. The thicknesses of the two layers are set to $0.5\lambda_0/\sqrt{\varepsilon'_{r1}} \simeq 100\,\mu$m and $0.25\lambda_0/\sqrt{\varepsilon'_{r2}} \simeq 15\,\mu$m, for the substrate and the superstrate, according to the design rules of [22], [23]. Through the application of (22), we obtained an equivalent PRS model with normalized admittance $\bar{Y}_s = 0.43 + j9.9$.

From the numerical dispersion analysis of both the SS-LWA and the equivalent PRS model (see Figs. 8(a) and (d), respectively), it is immediately seen that (22) is correctly modeling the effect of the superstrate layer. As for the previous case study, the radiation patterns over the principal planes as well as the 3-D pattern obtained through the full-wave simulation are reported respectively in Figs. 8(b)–(c) for the SS-LWA, and in Figs. 8(e)–(f), for the equivalent PRS model. The obtained radiation efficiencies for this case study are also listed in Table II for both the SS-LWA (second row of Table II) and the equivalent PRS model (third row of Table II). As is seen, even in this case, a very good agreement is obtained among analytical, numerical, and full-wave results, for both models.

C. PRS-based FPC-LWAs

PRS-based FPC-LWAs were originally proposed by G. von Trentini in the '50s [33], although a leaky-wave interpretation for the gain enhancement of these antennas was recognized only later [34], [35]. The PRS can take various forms [10], but here we consider homogenized PRSs, i.e., periodic arrangements of unit-cells with a period $p \ll \lambda_0$. In particular, a fishnet-like unit-cell as those proposed in [9] is selected as it fulfills the hypothesis of TE-TM equalization, and negligible spatial dispersion. The fishnet element can be

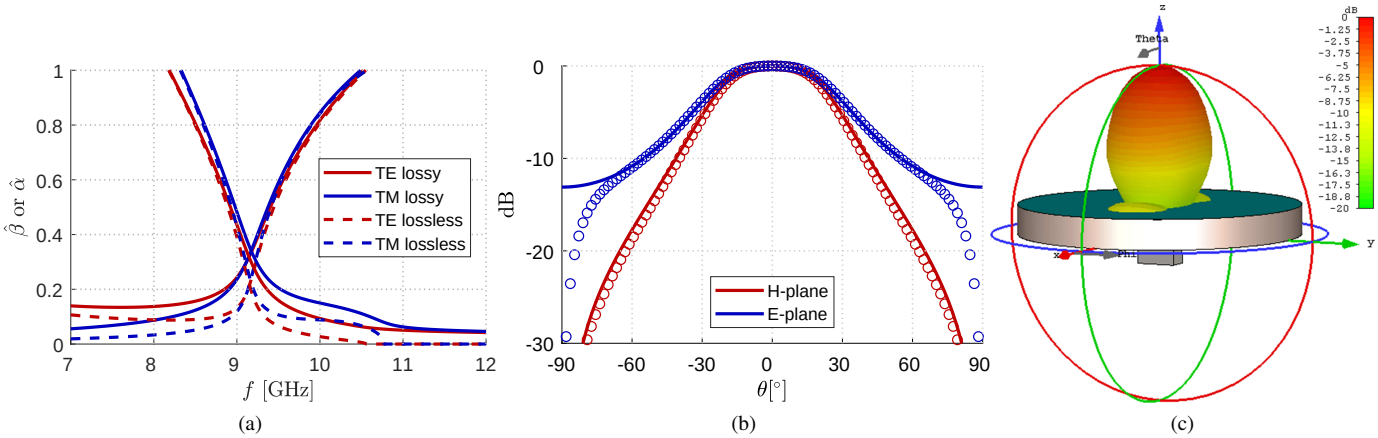

(a) (b) (c)

Fig. 9. Results for the case study of Subsection IV.C (PRS-based FPC-LWAs). (a)–(c) As in Figs. 7 and 8, but for the PRS-based FPC-LWA.

realized by etching crossed slots on a metallic plate. The length l and the width w of the slots can be tuned to synthesize the desired PRS admittance [9]. In this case study, a PRS based on a fishnet element with $p = 6$ mm, $l = 2.4$ mm, $w = 1.2$ mm is synthesized at 10 GHz through full-wave simulations (following the procedure outlined in [9], [36]), and leading to a normalized admittance $\bar{Y}_s = -j7.54$. As opposed to the design in [9], where Zeonor was used as a substrate thanks to its relatively low loss tangent at 1 THz, here we use a $\lambda/2$-thick FR-4 substrate ($\varepsilon_r' = 4.3$, $\tan\delta = 0.025$ [25, Material library]) due to its extensive use at microwave frequencies, and its relatively high dielectric losses.

As for the previous cases studies, results are reported in Fig. 9(a)–(c), showing the dispersion curves (Fig. 9(a)), the normalized radiation patterns over the principal planes (Fig. 9(b)), and the 3-D pattern (Fig. 9(c)). The obtained radiation efficiency is below 50%, and a very good agreement is obtained between analytical, numerical, and full-wave results (see the last row of Table II).

As a final remark, it is worth to comment the error that would be obtained by estimating the radiation efficiency η_r at broadside through $\alpha_{\rm rad}/\alpha$ (the old formula) instead of $(\alpha_{\rm rad}/\alpha)^2$ (the formula proposed here). Since $\eta_r < 1$, the old formula overestimates the correct value, leading to larger errors for lower radiation efficiencies. To give some numbers, the old formulas would predict radiation efficiencies of 64%, 78%, and 68%, for the case studies of IV-A, IV-B, and IV-C, respectively, whereas the full-wave simulations predict 39.7%, 62.8%, and 46.9%, respectively, in close agreement with the formulas proposed here (see Table II).

V. Conclusion

In this work, we extended the previous existing expressions for the evaluation of losses in leaky-wave antennas. As is known, the current formulas to evaluate the radiation efficiency required for the leaky-wave antenna to operate in the scanned-beam region. The theoretical analysis reported here has provided new formulas that allow for rigorously evaluating the losses in any traveling-wave antenna without any restriction to the radiating regime.

Moreover, the relevant case of Fabry-Perot cavity leaky-wave antennas radiating at broadside is discussed. Formulas are derived for an analytic and accurate evaluation of the radiation efficiency when a lossy PRS is employed in a Fabry-Perot cavity leaky-wave antenna: a case of great interest for THz designs, where material losses are no longer negligible.

In this regard, three relevant application examples are discussed: a graphene-based antenna and a substrate-superstrate antenna in the THz range, and a FPC-LWA based on a homogenized PRS in the microwave range. The first and the third structure are PRS-based leaky-wave antennas (a graphene sheet is actually modeled as a lossy PRS), thus it was possible to directly apply the analytical formulas derived here. Conversely, the substrate-superstrate antenna required an original analysis to prove the equivalence between a lossy superstrate layer and a lossy PRS. A simple formula has thus been obtained for correctly modeling a lossy superstrate layer through a complex-valued PRS impedance.

All the analytical contributions derived in this work have been validated with a comprehensive full-wave analysis of different structures.

It is expected that these results will provide an efficient tool for the performance evaluation of leaky-wave antenna designs in the microwave and (sub)-millimeter frequency band, as well as in the optical range.

Acknowledgments

The Author wishes to acknowledge Alessandro Galli and Paolo Burghignoli for having encouraged the writing of this manuscript, as well as for stimulating discussions on this and others leaky-wave topics.

Appendix

In [14], it was found that a $\lambda/4$-thick lossless dielectric layer placed on top of a grounded dielectric slab can accurately be modeled by a lossless sheet normalized admittance $\bar{Y}_s = j\bar{B}_s$ with B_s given by the formula:

$$\bar{B}_s = \sqrt{\varepsilon_r} \tag{24}$$

for broadside incidence (in [14], a more general formula is reported for the case of arbitrary incidence). This formula is obtained by equating the magnitude of the reflection coefficient $|\Gamma_1|$ (seen at the interface between the dielectrics of the SS-LWA), to that of the reflection coefficient $|\Gamma_2|$ (seen at the interface between the substrate and the PRS in the equivalent PRS model).

In general, $|\Gamma_1|$ and $|\Gamma_2|$ have the following expressions:

$$|\Gamma_1| = |(\bar{Y}_1 - \bar{Y}_1^+)/(\bar{Y}_1 - \bar{Y}_1^+)|, \tag{25}$$
$$|\Gamma_2| = |(\bar{Y}_1 - \bar{Y}_2^+)/(\bar{Y}_1 - \bar{Y}_2^+)|, \tag{26}$$

where $\bar{Y}_1$ is the normalized characteristic admittance in the substrate, whereas $\bar{Y}_1^+$ and $\bar{Y}_2^+$ are the input normalized admittances seen by looking upwards from the substrate-superstrate interface, and from the substrate-PRS interface, respectively.

Under the hypotheses of *i)* broadside incidence, *ii)* no dielectric losses, and *iii)* high reflectivity, i.e., $\varepsilon_{r2}/\varepsilon_{r1} \gg 1$ (where $\varepsilon_{r1(2)}$ is the relative permittivity of the substrate (superstrate)) for the SS-LWA, and $\bar{B}_s \gg 1$ for the PRS model, it was found in [14] that $\bar{Y}_1^+ \simeq \bar{Y}_2^2/\bar{Y}_0 \simeq \varepsilon_{r2}$, whereas $\bar{Y}_2^+ = \bar{Y}_0 + j\bar{B}_s \simeq 1 + j\bar{B}_s$, and consequently:

$$|\Gamma_1| \sim 1 - 2\bar{Y}_1/\bar{Y}_1^+ \sim 1 - 2\sqrt{\varepsilon_{r1}}/\varepsilon_{r2}, \tag{27}$$
$$|\Gamma_2| \sim 1 - 2\bar{Y}_1/\bar{B}_s^2 \sim 1 - 2\sqrt{\varepsilon_{r1}}/B_s^2. \tag{28}$$

Equation (24) is readily obtained by equating $|\Gamma_1| = |\Gamma_2|$, using the expressions above, i.e., (27)–(28).

When the hypothesis of no dielectric losses (viz., *ii)*) is removed, $\varepsilon_{r2} = \varepsilon'_{r2}(1 - j\tan\delta_{\varepsilon 2})$, where $\tan\delta_{\varepsilon 2}$ is the loss tangent of the superstrate. As a result, it is neither possible to assume $\bar{Y}_1^+ \simeq \bar{Y}_2^2/\bar{Y}_0$, nor possible to use a *lossless* PRS to model a *lossy* superstrate. While the expression of $|\Gamma_2|$ can be easily generalized for a lossy PRS by adding a real part to $\bar{Y}_s$ such that $\bar{Y}_s = \bar{G}_s + j\bar{B}_s$ and

$$|\Gamma_2| \sim 1 - 2\bar{Y}_1(1 + \bar{G}_s)/\bar{B}_s^2, \tag{29}$$

the derivation of $|\Gamma_1|$ in the lossy case requires a specific attention. As a matter of fact, when dielectric losses are introduced in the superstrate, the input admittance is no longer simply given by the quarter-wavelength transformation rule, but reads:

$$Y_1^+ = \bar{Y}_2 \frac{\bar{Y}_0 + j\bar{Y}_2 \tan(k_{x2}h)}{\bar{Y}_2 + j\bar{Y}_0 \tan(k_{x2}h_2)}, \tag{30}$$

where $k_{x2} = k_0\sqrt{\varepsilon_{r2} - k_z^2}$ and $h_2 = 0.25\lambda_0\sqrt{\varepsilon'_{r2}}$, are the vertical wavenumber and the thickness of the superstrate (λ_0, being the operating wavelength). For broadside incidence, Y_1^+ simplifies as

$$Y_1^+ = \sqrt{\varepsilon_{r2}} \frac{1 + j\sqrt{\varepsilon_{r2}}\tan\left[\frac{\pi}{2}\sqrt{1 - j\tan\delta_{\varepsilon 2}}\right]}{\sqrt{\varepsilon_{r2}} + j\tan\left[\frac{\pi}{2}\sqrt{1 - j\tan\delta_{\varepsilon 2}}\right]}. \tag{31}$$

For $\delta_{\varepsilon 2} \to 0$, we recover the previous result, whereas under the hypothesis of small losses ($\delta_{\varepsilon 2} \simeq 0$), the tangent function of a complex argument $\tan z = \tan(x + jy)$ can be approximated to $\tan z \sim j\coth y$ for $x \to \pi/2$ and $x \gg y$, thus leading to

$$Y_1^+ \simeq \sqrt{\varepsilon_{r2}} \frac{1 + \sqrt{\varepsilon_{r2}}\coth\left[\frac{\pi}{2}\sin(\delta_{\varepsilon 2}/2)\right]}{\sqrt{\varepsilon_{r2}} + \coth\left[\frac{\pi}{2}\sin(\delta_{\varepsilon 2}/2)\right]}. \tag{32}$$

For small losses, and to a first-order approximation, we have $\coth x \gg 1$, $\varepsilon_{r2} \simeq \varepsilon'_{r2}$, $\tanh x \sim x$, and then (32) can be further simplified to

$$Y_1^+ \sim \frac{\varepsilon'_{r2}}{1 + \sqrt{\varepsilon'_{r2}}\frac{\pi}{2}\sin(\delta_{\varepsilon 2}/2)}. \tag{33}$$

Equation (33) is our sought expression and since $Y_1^+ \in \mathbb{R}$, it can directly be replaced in (27) leading to:

$$|\Gamma_1| \sim 1 - 2\frac{\bar{Y}_1}{\varepsilon'_{r2}}\left(1 + \sqrt{\varepsilon'_{r2}}\frac{\pi}{2}\sin(\delta_{\varepsilon 2}/2)\right). \tag{34}$$

A comparison of (34) and (29) furnishes an infinite set of pairs $(\bar{G}_s, \bar{B}_s)$ that satisfy the equation $|\Gamma_1| = |\Gamma_2|$. However, in the limit of no losses, i.e., for $\delta_{\varepsilon 2} \to 0$ and $\bar{G}_s \to 0$, (34)–(29) reduce to (27)–(28), and hence the imaginary part of the normalized admittance $\bar{B}_s$ is still determined by (24). Therefore, by enforcing $\bar{B}_s = \sqrt{\varepsilon'_{r2}}$ in (29), and equating $|\Gamma_1| = |\Gamma_2|$, the real part of the normalized admittance reads

$$\bar{G}_s \sim \sqrt{\varepsilon'_{r2}}\frac{\pi}{2}\sin(\delta_{\varepsilon 2}/2), \tag{35}$$

and equation (22) is finally obtained. We also note that $\bar{G}_s \geq 0$, being $\delta_{\varepsilon 2} \in [0, \pi/2]$, as it should be for a passive material with $\varepsilon'_r > 0$ (the equality sign holds for $\delta_{\varepsilon 2} = 0$).

REFERENCES

[1] Y. Liao, E. de Freitas Rocha Loures, and F. Deschamps, "Industrial internet of things: A systematic literature review and insights," *IEEE Internet of Things Journal*, vol. 5, no. 6, pp. 4515–4525, 2018.
[2] P. Smulders, "The road to 100 Gb/s wireless and beyond: basic issues and key directions," *IEEE Commun. Mag.*, vol. 51, no. 12, pp. 86–91, 2013.
[3] D. R. Jackson and A. A. Oliner, "Leaky-Wave Antennas," in *Modern Antenna Handbook*, C. A. Balanis, Ed. New York, NY, USA: John Wiley & Sons, 2011, ch. 7.
[4] A. Hosseini, F. Capolino, and F. De Flaviis, "Gain enhancement of a V-band antenna using a Fabry-Pérot cavity with a self-sustained all-metal cap with FSS," *IEEE Trans. Antennas Propag.*, vol. 63, no. 3, pp. 909–921, 2015.
[5] H. Attia, M. L. Abdelghani, and T. A. Denidni, "Wideband and high-gain millimeter-wave antenna based on FSS Fabry–Pérot cavity," *IEEE Trans. Antennas Propag.*, vol. 65, no. 10, pp. 5589–5594, 2017.
[6] L. Chang, Z. Zhang, Y. Li, S. Wang, and Z. Feng, "60-Ghz air substrate leaky-wave antenna based on MEMS micromachining technology," *IEEE Trans. Comp., Pack. Technol.*, vol. 6, no. 11, pp. 1656–1662, 2016.
[7] X.-C. Wang, W.-S. Zhao, J. Hu, and W.-Y. Yin, "Reconfigurable terahertz leaky-wave antenna using graphene-based high-impedance surface," *IEEE Trans. Nanotech.*, vol. 14, no. 1, pp. 62–69, 2015.
[8] W. Fuscaldo, P. Burghignoli, P. Baccarelli, and A. Galli, "Graphene Fabry-Perot cavity leaky-wave antennas: Plasmonic versus nonplasmonic solutions," *IEEE Trans. Antennas Propag.*, vol. 65, no. 4, pp. 1651–1660, Apr. 2017.
[9] W. Fuscaldo, S. Tofani, D. C. Zografopoulos, P. Baccarelli, P. Burghignoli, R. Beccherelli, and A. Galli, "Systematic design of THz leaky-wave antennas based on homogenized metasurfaces," *IEEE Trans. Antennas Propag.*, vol. 66, no. 3, pp. 1169–1178, Mar. 2018.
[10] W. Fuscaldo, S. Tofani, P. Burghignoli, P. Baccarelli, and A. Galli, "Terahertz leaky-wave antennas based on metasurfaces and tunable materials," in *Metamaterials and Metasurfaces*, J. Canet-Ferrer, Ed. IntechOpen, 2018, pp. 93–116.
[11] G. Lovat, P. Burghignoli, and D. R. Jackson, "Fundamental properties and optimization of broadside radiation from uniform leaky-wave antennas," *IEEE Trans. Antennas Propag.*, vol. 54, no. 5, pp. 1442–1452, May 2006.
[12] C. Di Nallo, F. Frezza, A. Galli, and P. Lampariello, "Rigorous evaluation of ohmic-loss effects for accurate design of traveling-wave antennas," *J. Electromagn. Waves Appl.*, vol. 12, no. 1, pp. 39–58, 1998.

[13] J. Gómez-Tornero, G. Goussetis, and A. Álvarez-Melcón, "Correction of dielectric losses in practical leaky-wave antenna designs," *J. Electromagn. Waves Appl.*, vol. 21, no. 8, pp. 1025–1036, 2007.
[14] T. Zhao, D. R. Jackson, J. T. Williams, and A. Oliner, "Simple CAD model for a dielectric leaky-wave antenna," *IEEE Antennas Wireless Propag. Lett.*, vol. 3, no. 1, pp. 243–245, 2004.
[15] G. Minatti, E. Martini, and S. Maci, "Efficiency of metasurface antennas," *IEEE Trans. Antennas Propag.*, vol. 65, no. 4, pp. 1532–1541, 2017.
[16] A. Oliner and A. Hessel, "Guided waves on sinusoidally-modulated reactance surfaces," *IRE Trans. Antennas Propag.*, vol. 7, no. 5, pp. 201–208, 1959.
[17] T. Tamir and A. A. Oliner, "Guided complex waves. Part 1: fields at an interface," *Proc. IEE*, vol. 110, no. 2, pp. 310–324, Feb. 1963.
[18] ——, "Guided complex waves. Part 2: relation to radiation patterns," *Proc. IEE*, vol. 110, no. 2, pp. 325–334, Feb. 1963.
[19] A. A. Oliner and D. R. Jackson, "Leaky-Wave Antennas," in *Antenna Engineering Handbook*, J. L. Volakis, Ed. New York, NY, USA: McGraw-Hill, 2007, ch. 11.
[20] D. M. Pozar, *Microwave Engineering*. Hoboken, NJ, USA: John Wiley & Sons, 2009.
[21] A. Ip and D. R. Jackson, "Radiation from cylindrical leaky waves," *IEEE Trans. Antennas Propag.*, vol. 38, no. 4, pp. 482–488, Apr. 1990.
[22] D. R. Jackson and N. G. Alexópoulos, "Gain enhancement methods for printed circuit antennas," *IEEE Trans. Antennas Propag.*, vol. 33, pp. 976–987, Sep. 1985.
[23] D. R. Jackson and A. A. Oliner, "A leaky-wave analysis of the high-gain printed antenna configuration," *IEEE Trans. Antennas Propag.*, vol. 36, no. 7, pp. 905–910, Jul. 1988.
[24] V. Galdi and I. M. Pinto, "A simple algorithm for accurate location of leaky-wave poles for grounded inhomogeneous dielectric slabs," *Microw. and Opt. Technol. Lett.*, vol. 24, no. 2, pp. 135–140, 2000.
[25] "CST products Darmstadt, Germany, 2016." [Online]. Available: http://www.cst.com
[26] "VDI Virginia Diodes, Inc., Waveguide band designations." [Online]. Available: http://vadiodes.com/VDI/pdf/waveguidechart200908.pdf
[27] J. M. Jornet and I. F. Akyildiz, "Graphene-based plasmonic nano-antenna for terahertz band communication in nanonetworks," *IEEE J. Sel. Areas Commun.*, vol. 31, no. 12, pp. 685–694, 2013.
[28] G. W. Hanson, "Dyadic Green's functions and guided surface waves for a surface conductivity model of graphene," *J. App. Phys.*, vol. 103, no. 6, p. 064302, 2008.
[29] G. Ni, A. McLeod, Z. Sun, L. Wang, L. Xiong, K. Post, S. Sunku, B.-Y. Jiang, J. Hone, C. Dean *et al.*, "Fundamental limits to graphene plasmonics," *Nature*, vol. 557, no. 7706, p. 530, 2018.
[30] M. Naftaly and R. E. Miles, "Terahertz time-domain spectroscopy for material characterization," *Proc. IEEE*, vol. 95, no. 8, p. 1658, 2007.
[31] P. A. George, W. Hui, F. Rana, B. G. Hawkins, A. E. Smith, and B. J. Kirby, "Microfluidic devices for terahertz spectroscopy of biomolecules," *Opt. Express*, vol. 16, no. 3, pp. 1577–1582, 2008.
[32] P. H. Bolivar, M. Brucherseifer, J. G. Rivas, R. Gonzalo, I. Ederra, A. L. Reynolds, M. Holker, and P. de Maagt, "Measurement of the dielectric constant and loss tangent of high dielectric-constant materials at terahertz frequencies," *IEEE Trans. Microw. Theory Tech.*, vol. 51, no. 4, pp. 1062–1066, 2003.
[33] G. von Trentini, "Partially reflecting sheet arrays," *IRE Trans. Antennas Propag.*, vol. 4, no. 4, pp. 666–671, 1956.
[34] A. P. Feresidis and J. C. Vardaxoglou, "High gain planar antenna using optimised partially reflective surfaces," *IEE Proc. Microwaves, Antennas Propag.*, vol. 148, no. 6, pp. 345–350, 2001.
[35] D. R. Jackson, P. Burghignoli, G. Lovat, F. Capolino, J. Chen, D. R. Wilton, and A. A. Oliner, "The fundamental physics of directive beaming at microwave and optical frequencies and the role of leaky waves," *Proceedings of the IEEE*, vol. 99, no. 10, pp. 1780–1805, 2011.
[36] O. Luukkonen, C. Simovski, G. Granet, G. Goussetis, D. Lioubtchenko, A. V. Raisanen, and S. A. Tretyakov, "Simple and accurate analytical model of planar grids and high-impedance surfaces comprising metal strips or patches," *IEEE Trans. Antennas Propag.*, vol. 56, no. 6, pp. 1624–1632, Jun. 2008.

Walter Fuscaldo (S'15–M'18) received the B.Sc. and M.Sc. (cum laude) degrees in Telecommunications Engineering from Sapienza University of Rome, Rome, in 2010 and 2013. In 2017, he received the Ph.D. degree (cum laude and with the *Doctor Europaeus* label) from both the Department of Information Engineering, Electronics and Telecommunications (DIET) and the Institut d'Électronique et de Télécommunications de Rennes (IETR), Université de Rennes 1, Rennes, France, under a cotutelle agreement between the institutions.

In 2014, 2017, and 2018, he was a Visiting Researcher with the NATO-STO Center for Maritime Research and Experimentation, La Spezia, Italy. In 2016, he was a Visiting Researcher with the University of Houston, Houston, TX, USA. His current research interests include propagation of leaky waves, surface waves and surface plasmon polaritons, analysis and design of leaky-wave antennas, generation of limited-diffraction limited-dispersion electromagnetic waves, millimeter-wave focusing systems, graphene electromagnetics, metasurfaces, and THz antennas.

Dr. Fuscaldo was a recipient of the Yarman-Carlin Student Award at the IEEE 15th Mediterranean Microwave Symposium in 2015, and he was awarded the Young Engineer Prize for the Best Paper presented at the 46th European Microwave Conference in 2016, the IEEE AP-S Student Award, Chapter Center-Southern Italy in 2017, the Best Paper in Electromagnetics and Antenna Theory at the 12th European Conference on Antennas and Propagation in 2018, the "Barzilai Prize" for the best scientific work of under-35 researchers at the 22th National Meeting of Electromagnetics, and the Young Scientist Award at the 41st PhotonIcs and Electromagnetics Research Symposium. He received the Publons Peer Review Award 2018 for placing in the top 1% reviewers in Engineering on Publons' global reviewers database, determined by the number of peer review performed during the 2017–2018 Award year. He is currently an Associate Editor of the journal *IET Microwaves, Antennas and Propagation*.